Experimental study of nonlinear interaction of plasma flow with charged thin current sheets: 2. Hall dynamics, mass and momentum transfer.

S. Savin (1), E. Amata (2), M. F. Marcucci (2), M. Andre (3), M. Dunlop (4), Y. Khotyaintsev (3), P.M.E. Decreau, J.L. Rauch, J.G. Trotignon, (5), J. Buechner (6), J. Blecki (7), A.M.Buckley, T.Carozzi, M.P.Gough (8), A. Skalsky, S. Romanov, L. Zelenyi (1), A. Volosevich (9), H. Rème(10)

(1) Russia IKI, Moscow (ssavin@iki.rssi.ru), (2) IFSI, Roma, Italy, (3) IRFU, Uppsala, Sweden, (4) RAL, UK, (5) LPCE, Orleans, France; (6) MPSP, Germany, (7) SRC, Warsaw, Poland, (8) U. Sussex, UK, (9) U. Mogilev, Belarus (10) CESR, Toulouse, France.

ABSTRACT

Proceeding with the analysis of Amata et al., (2005), we suggest that the general feature for the local transport at a thin magnetopause (MP) consists of the penetration of ions with gyroradius > MP width, and, in crossing it, the transverse potential difference at the thin current sheet (TCS) is acquired by these ions, providing field-particle energy exchange without parallel electric fields. It is suggested that a part of the surface charge is self-consistently produced by deflection of ions in the course of inertial drift in the non-uniform electric field at MP.

Consideration of the partial moments of ions with different energies demonstrates that the larger-gyroradius protons carry the normal to MP flux of about 20% of the total flow in the plasma jet under MP. Comparison of the ion transverse velocity and the cross-field drift speed in the jet inside MP, reveals an ion velocity excess of ~ 25%, which is accounted for the contribution of the finite-gyroradius inflow across MP. A linkage through the TCS between different plasmas results from the momentum conservation of the higher-energy ions. If the finite-gyroradius penetration occurs along the upstream MP throughout ~1.5 R_E, then it can completely account for the formation of the jet under MP. To provide the downstream acceleration of the flow near MP via the cross-field drift, the weak magnetic field is rotated from its nearly parallel direction in the unperturbed flow toward being almost perpendicular to the normal electric field at MP. We discuss a deceleration of the higher-energy ions in the MP normal direction due to the interaction with finite-scale electric field bursts in the magnetosheath flow frame, equivalent to collisions, and providing a charge separation. Further cascading towards electron scales is supposed to be due to unstable parallel electron currents, neutralizing the potential differences, either resulting from the ion- burst interactions or from the inertial drift.

The Poynting vector infers irradiating waves from MP into the upstream region with the waves triggering impulsive downstream flows, carrying up to 1/3 of the extra flux, providing the local flow balance and the outward movement of MP. Equalizing of the transverse electric field inside the MP TCS by the Hall term in the Ohm's law implies a separation of the different plasmas primarily by the Hall current, driven by the respective part of the TCS surface charge.

INTRODUCTION.

We proceed with analysis of the transport processes and mechanisms for plasma jets acceleration at a thin current sheet (TCS) observed on February 13, 2001, which has been identified with the magnetopause (MP) in the companion paper Amata et al., (2005) from Cluster data (cited further as '[A]'). In this paper we propose an explanation for the different directions of the local normal from both minimum variance of the magnetic field and from maximum variance of the electric field versus direction of the MP motion from the observed time delays on 4 spacecraft (cf. Dunlop et al., 2005), suggesting that the motion of the indented MP is defined by non-local properties of the near-cusp region as an entity. We compare the ion velocity with the cross-field drift velocity, demonstrating a systematic deficit of the drift speed of ~ 25% only in the tailward plasma jet just inside the TCS.

The Hall dynamics of the thin MP current sheet is outlined. Previous studies of data from Interball-1, Polar and Cluster (Nikutowski et al., 1998, 1999, Mozer et al., 2003, Vaivads et al., 2004), has been mostly limited to the comparison with models of stationary X-line macro reconnection. In the TCS the frozen-in condition is violated due to the small current

scale, which can be described not only in reconnection-like approximations, but also in terms of gyro-viscosity (Stasiewicz, 1994, Hultqvist et al., 1999). Belmont and Rezeau (2001) use the term 'micro reconnection' for similar effects of Alfven waves on the magnetic flux erosion. The Hall dynamics of the charged TCS, might include transient (and multiple) X-, Y-, O-lines etc. as particular scenarios for the current sheet evolution (see e.g. Syrovatskii, 1971, Hultqist et al., 1999, Zelenyi et al. 2002, Silin and Buechner, 2003, Savin et al., 2004b, 2005a). For a simple model Moser et al., (2003) demonstrate that the Hall dynamics per se can explain local plasma structuring without local reconnection features (e.g. parallel electric fields). We propose that electrons with large thermal speeds can provide surface charges at the TCS moving along field lines. The surface charges support diamagnetic currents, separating different plasmas. In turn, the potential difference for driving the field-aligned electron current might result from inertial drift of the incident MSH ions in the non-uniform electric field of the surface charge, seen in the frame of bulk motion by the MSH plasma; and the inertial drift results in ion separation from electrons (cf. Genot et al., 2004, Savin et al., 2004a, 2005a). Recent papers, claiming crossings of a diffusion region (e.g. Vaivads et al., 2004, Mozer et al., 2003), in reality confirm the Hall ion dynamics in TCS and show the existence of substructures of electron-gyroradius (inertial-length) scales, the presence of which automatically implies breaking of frozen-in conditions for electrons (cf. Savin et al., 1998, Andre et al., 2004). Those features naturally are present in reconnection models, while they are also characteristic of a kinetic TCS without reconnection (see e.g. Silin and Buechner, 2003). Filamented electron beams of electron scales also account for the neutralization of the potential difference, generated by the charge separation through inertial drift (Genot et al., 2004). The inertial drift in standing electric wave-packets at the outer border of the MP boundary layer is able to accelerate the structured jets up to magnetosound and highly super-Alfvenic velocities, and the jet dynamic pressure can largely exceed that of the magnetic one at a downstream MP (Savin et al., 2004a, 2005b).

We apply the inertial drift and Hall physics for interpretation of the data in the MP vicinity, compare with a reconnection input into the dynamics, mass and momentum balance at MP. It is demonstrated that the finite-gyroradius effect can account for a substantial mass and momentum transfer across MP. We suggest a non-reconnection mechanism for the formation of plasma streams near MP: the larger-energy ions conserve their momentum parallel to MP during the motion across MP in the high-beta plasma, resulting in the motion of the inner plasma without an annihilation of the magnetic field, i.e without the macro reconnection.

Plasma inflow and momentum balance.

In this second companion paper we proceed with the discussion of the thin (~ proton gyroradius) plasma separatrix between MSH and magnetospheric plasmas in boundary layers (see Amata et al., 2005, [A]), shifting the stress towards the data interpretation in the light of plasma and momentum transport across the MP.

We have demonstrated in Fig. 1 [A] that the largest flow bursts near the MP occur in the perpendicular ones in contrast to the GDCF model prediction and to unperturbed flows (see [A] and Savin et al., 2002). Thus the perpendicular flows are of general importance for the mass balance near MP.

To estimate how finite-gyroradius effecst affect a flow balance near MP, we compare the drift velocity $\mathbf{V}_D = c[\mathbf{E}x\mathbf{B}]$, which can be studied at the sampling rate of ~ 25 Hz (magnetic field data has been interpolated to that of electric field), and ion velocity (also interpolated to the electric field sampling), perpendicular to magnetic field, $\mathbf{V}_{perp}$ in Fig. 1, where one can see a general correspondence of the two values. This occurs in spite of a non-equilibrium plasma with co-existing ion distributions with different moments (see Fig. 2 [A]) which should not follow single-fluid Ohm equation (cf. Hultqvist et a., 1999). In the dominant Y-component there is a small systematic difference between $\mathbf{V}_{perp}$ and $\mathbf{V}_D$ with average values and standard deviations for the MSH interval 19:55:00-20:00:40 UT being V_{yperp}-V_{yd} ~ 3 +/-19 km/s, while V_{yperp}-V_{yd} ~ -13 +/-31 km/s at the total interval 19:55-20:05 UT (see the bottom of Fig. 1, at the left). Inside the magnetosphere at 20:04-20:05 UT the shift in V_{yperp}-V_{yd} ~ -20 +/-14 km/s is due to different offsets in the E_x component of the electric-field instrument in the dilute magnetospheric plasma (the offset difference is much smaller for other electric field components); for the jet under MP at 20:00:50-20:02:00 UT (marked by the violet bar at the right bottom side of Fig. 1) $|\mathbf{V_{perp}}-\mathbf{V_d}|$ ~ 64 +/-45 km/s, i.e. ~31% of the total ion velocity in this interval. In the jet the relative difference is even larger in X and Z components. The $\mathbf{V}_D$ is smaller in absolute value as if an inflow through the boundaries substantially contributes into the flow balance. The minimum contribution of the inflow can be estimated as the difference between the jet and magnetospheric values in the dominant Y component (in the jet the plasma density is high, so that the offset in E_x is close to the MSH one), i.e. 23% from the total flow in the jet. So, we take 25% as a rough estimate for the difference between the measured perpendicular flow and the contribution of electric cross-field drift into the jet under MP.

To facilitate further analysis of the thin nonlinear structure, TCS, we calculate the partial moments for ions with energy larger than a chosen value in the spacecraft frame. However this might pose certain errors as we cannot calculate these moments in a plasma bulk frame for two reasons: (i) the flow velocity changes much on each time step of 4 s, while we need to compare the input in the flow from ions with different energies over the interval of several minutes; (ii) the plasma appears to be a non-equilibrium one with co-existing ion populations with different moments (see Figs. 2, 4, 5 and 6 [A] and related discussion in [A]), that, in principle, require extracting separate moments for each ion population and a comparison with respective multi-fluid equations (planned for a future paper).

In Fig. 2 we display total density (thin blue curve), compared with the GDCF prediction (thick blue line). In general they are in agreement until ~ 20:50 UT, when the total density starts to fluctuate and finally drops at ~ 20:07 UT toward the outer cusp value. Cargill et al., (2004) attribute the region after 20:07 UT to 'lobes'; but both density of ~ 13 cm^{-3} (up to 20:13 UT) and ion spectrogram in Cargill et al., (2004) correspond rather to the mantle cusp, and the remainder of the time period in Fig. 1 [A] we attribute to a mantle. Inside the region of density fluctuations (19:50-20:07 UT) ions of > 1 keV are intensified, having maxima in the jet edges at 19:50 and 20:01 UT. The latter is just inside MP, preceded by the sharp maximum outside MP, which corresponds to MSH flow, piled up by the MP outward motion. Density of ions with energy > 196 eV generally follows the total density outside MP and the density of the more energetic ions inside MP (cf. Fig. 4b [A]).

In Fig. 3 we magnify the densities' behavior at MP (top, note replacing energies '> 196 eV' by '>300 eV' for comparison with Fig. 4b [A]) and add respective ion-flow components in GSE frame (also colored according to the carrier energy); MP and nearest 4-second intervals of the CIS scans are marked by vertical green lines. Just outside MP the ion flux is carried by the colder ions with small gyroradius. The large-gyroradius ions (energy > 1 keV) carry up to 60% of the flux in the jet inside MP. Note inward large-gyroradius flow nV_{ix} (marked by blue-red dashed line), which constitutes ~ 20% of the total flow in the inner jet. This inward flux should not feel the small-scale MP current sheet, i.e. it gives the lower-limit estimate for the local influx. The intermediate-energy ions could also provide an input into the inflow, while the minimum influx at 19:54 UT is defined largely by the large-gyroradius influx. At the magnetospheric border of the inner jet (after 20:02 UT) there is a vanishing X-component of inflow (the normal from magnetic field minimum variance $\mathbf{N_B}$ is close to X, see Fig. 8 [A] and related discussions in [A]). Thus from the necessary mass-conservation in an almost incompressible plasma, we suggest that this inflow provides a local source for the jet. Its minimum contribution (estimated above as ~ 20%) agrees fairly well with ~ 25% of the ion velocity ($\mathbf{V}_{perp}$) excess over the electric-drift velocity ($\mathbf{V}_D$) in Fig. 1. From the MP outward speed and duration of the inner plasma jet we can estimate its width to be ~ 2000 km, which yields a proxy for the scale along MP of ~1.5 R_E, at which the jet can be formed uniquely by the inflow from finite-gyroradius effects (providing similar MP structure upstream from the Cluster crossing). The 1.5 R_E is almost one half of the characteristic dimension along MP of 'plasma balls' (i.e. the large-scale depletions in magnetic field, see Fig. 1 [A], cf. Savin et al., 2002, 2005a); thus we regard the finite-gyroradius effect as a major plasma source for the inner jet (other sources are discussed in the 'Discussion' section).

Another interesting feature, visible in Fig. 3, is conservation of the dominant nV_z flux across MP for ions with energy > 300 eV. These ions carry the major ion flux at MP from both sides. We illustrate this process in Fig. 4. In the high-beta situation, ions interpenetrated across MP due to the finite-gyroradius effect should nearly conserve their momentum parallel to MP. Just ahead of MP the parallel flow dominates (see Figs. 1 and 2 [A]), and its higher energy part does not feel the TCS, while the flow becomes the perpendicular one inside MP. For the $\beta>>1$ there, this flow moves the inner magnetic field downstream and contributes to the respective electric field component along the MP normal (see the negative spike in E_x in Figs. 1, 3, 7 [A] and 7). Actually, as we've mentioned above, the electric field should be calculated from multi-fluid equations (at least for two ion sub-populations). This exchange of momentum across TCS provides effective gyro-viscosity, which automatically results in the magnetic flux diffusion across MP (see e.g. Hultqvist, et al., 1999 and references therein). Another consequence of the exchange by the parallel momentum inside the 'plasma ball' would be a pumping of the inner magnetic field downstream, that enforces the magnetic field minimum over the cusps and, probably, constitutes one of general mechanisms for creating of the large-scale diamagnetic cavities - 'plasma balls' (cf. Savin et al., 2005a).

We now consider the contributions of wavy and quasi DC electric fields to the flow balance. In Fig. 5 we present GSE vectors of the electric field from Cluster 1 in a MSH-flow frame, moving at $\mathbf{V_{MSH}}$ = (-45, -90, -150) km/s; of magnetic field; of ion velocity; of Poynting flux; of vector of electric drift velocity; and finally Poynting flux projections onto the average normal from magnetic minimum variance analysis $\mathbf{N_B}$ (P2001_N_B, see Cargill et al., 2004) and onto the normal from the electric field maximum variance $\mathbf{N_E}$ (P2001_N_E, see [A]). Further in the text we use the notation $\mathbf{E}`$ for the electric field components in the MSH frame. The unperturbed $E`_x$ and $E`_y$ at the left side of Fig. 5 are close to zero, inferring for these components that the chosen particular value of $\mathbf{V_{MSH}}$ is a good proxy for transformation into the

MSH-flow frame for the total time interval; $E`_z$ at the left side of Fig. 5 has a DC offset, requiring a corresponding change of the MSH speed for the data transformation at the time interval beginning, but we neglect this offset relative to strong disturbances, visible in the middle of Fig. 5, generally in $E`_x$. So, the transformation into a MSH frame demonstrates that the incident ions are affected mainly by the $E`_x$ component, which is close to the MP normal (see discussion in [A]). Note that electric field at TCS is diminished in this frame, but the transformation used has no explicit sense under MP, which partially reflects the incident flow and partially transfers it (see discussion of Figs. 2 and 4 [A]).

The main input of the quasi DC electric field into the flow balance near MP is an acceleration of the plasma downstream, mainly in the -Z direction via the cross-field drift (see bottom curves). Remember, the strong positive $E`_x$ disturbances have a local origin, in contrast to the global GDCF predictions (see Fig. 1 [A] and Fig. 2 and related discussions above). The Poynting flux P_z component demonstrates that waves accelerate the plasma in the same direction, the similar behavior of P_z and V_{dz} conforms to transport of the disturbances downflow by the average plasma flux. Averaged V_{dz} at the interval of maximum drift 20:00:25-20:00:50 UT gives 91 km/s with a standard deviation of 39 km/s. As this averaging includes the input of the wavy spikes, we attribute ~ 75 km/s to the average cross-field drift, i.e. ~ 1/3 of the accelerated flow should in this case be due to the wavy input. The positive projections of Poynting flux onto the normals (pointed sunward) and positive P_x demonstrate that the waves propagate upstream, being most probably reflected from the MP (cf. Belmont and Rezeau, 2001 and Savin et al., 2005a) or emitted by the jet. V_{dy} outside MP is pointed in the +Y direction (i.e. along the smooth MP, see Fig. 6 and related discussion below), while inside MP it is along -Y axis, presumably due to the opposite normal electric field from different MP sides. It appears strange that the wavy disturbances (P_y) outside MP propagate in the opposite direction relative to the main outer V_{dy}, i.e. along -Y axis, as the waves inside MP do, and a correlation of the latter with V_y (dashed line) points to transport of the inner disturbances downstream by the jet. As the inner disturbances have the positive P_x and normal components, they should represent a source for the outer ones. Another reason for the outlined behavior would be guiding of the smaller-scale disturbances by the cusp throat, which has the opposite curvature compared to that of the smooth MP (see Fig. 6 and discussions below). We have checked that the Poynting flux and drift velocity behave similarly to that in the middle of Fig. 5 since ~ 19:56 UT, i.e. when E_x departs from the GDCF predictions (cf. [A]).

Quantitative impact of finite-gyroradius effects on the transport

In this section we discuss possible applications and consequences of finite-gyroradius effects and the local DC and AC electric fields, described above, to transport processes and MP dynamics.

The picture of the global configuration on February 13, 2001 at negative (anti-sunward) magnetic dipole tilt is rather typical with the MP separating MSH and heated plasma into outer cusp - 'plasma ball' (Savin et al., 2002a, 2005a). This is namely the situation of direct plasma-plasma interaction, while at the lower latitudes the plasma interacts with the magnetic barrier. The strong fluctuations between stagnant MSH and outer cusp in the cases of Savin et al., (2001) isolate them, while in our case a 'plasma ball' represents the interior large-scale reservoir for magnetospheric plasma.

First of all, it should be remembered that at the high-latitude MP we often deal with interaction of a high-beta incident plasma with a higher-beta one (cf. Savin et al., 2004a-b, 2005a-b, Lavraud et al., 2002, [A]). Thus, the magnetic forces are small and in a collisionless plasma the general plasma-plasma interactions involve electric fields, either (quasi) DC or wavy. In the fortunate case under study, the DC electric field in front of MP clearly differs from the normal electric field, which would be induced by the equilibrium gasdynamic flow (see differences in the measured and predicted by GDCF values of E_x in Fig. 1 [A] and 2).

A reason for the electric field departure from the model should be the MP deformation compared to the smooth MP in the GDCF model, being symmetric relative to the Sun-Earth axis. This is illustrated by the departure from the model normal (see Cargill et al., 2004) $\mathbf{N_{mod}}$ = (0.6, 0.15, -0.75) of both the average normal, deduced both from minimum variance analysis of magnetic field $\mathbf{N_B}$ and from the direction of maximum electric-field variance $\mathbf{N_E}$, strongly towards X axis. We verified that the minimum-variance direction on 200-second intervals departs from the $\mathbf{N_{B3}}$ ~ (0.97; -0.19; -0.15) (Cluster 3 normal from minimum variance analysis at 19:58:47-20:02:07 UT, see [A]) by less than 25 degrees since 19:42 UT that can be accounted for by control of the flow by the indented MP throughout this time interval, i.e. the MP indentation is rather a stationary feature and the direction of $\mathbf{N_{B3}}$ is not due to a temporal surface wave (cf. Dunlop et al., 2005, Cargill et al., 2004, Savin et al., 1998, 2004b,2005b). We illustrate the indented MP geometry in the Insert A of Fig. 6, and the deflected $\mathbf{N_{B3}}$ corresponds to the 3d and 4th blue vectors from the bottom. Returning to the normal electric field, inside the MP indentation the flow should be decelerated in the -X direction, but could be accelerated in the -Z direction to provide an equilibrium plasma outflow from the indentation. The enlarged (reduced) $E`_x$ at MP could serve to balance the upstream inflow by extra acceleration (deceleration) of the plasma downstream. To check this

option, we compare our data with a realistic gas-dynamic model with MP, determined from local pressure balance, in a future paper. A systematic disagreement of the measured and GDCF B_x is expected as a consequence of the normal departure from that of smooth MP: the magnetic field lines near MP should tend to elongate the MP (cf. Dunlop et al., 2005).

As mentioned above, another source for the local DC normal field is the outward movement of MP and boundary layers at velocities of ~ 30-40 km/s, and the MP, moving sunward, can remove an upstream plasma by accelerating it along MP downstream by means of an extra normal electric field. Fig. 5 confirms this suggestion by demonstrating the dominant negative component V_{dz} of the cross-field velocity (cf. Fig. 6); also seen is the positive drift in the +Y direction, which is probably a by-product of the normal electric field, dependent on the IMF direction. In the middle of Fig. 5 the drift quasi DC component constitutes ~ 60% of the simultaneous ion flow and ~ 80% of the unperturbed flow at 20:00:10 UT, i.e. the DC cross-field drift constitutes the major part of the flow in front of the moving MP. This is also the case just inside MP in the main jet (at ~ 20:01 UT).

We have discussed in [A] that the largest flow bursts near the MP are mostly the perpendicular ones in contrast to the GDCF prediction and to the unperturbed MSH flows (see Fig. 1 [A]). This suggests an 'active' role for the normal electric field in the MP vicinity in the regulation of the plasma flow balance. Remembering the smallness of the magnetic energy density, we make the following logistic step: we propose that the magnetic field deflection in the outer MP boundary layer results from the interaction of incident flow, streamlining around the high-beta obstacle ('pre-existed' plasma in Lavraud et al., 2002 or 'plasma ball' in Savin et al., 2004a, 2005a,b), with the normal electric field, supposed to be produced by the surface charge(s) at the MP current sheet(s). I.e. in the high-beta interaction a weak magnetic field should fit to the 'external' flow and 'external' electric field, in contrast to the flow interaction with a magnetic barrier (with dominating magnetic pressure) at lower latitudes, where the normal electric field is generally induced by the external flow at the fixed MP current sheet (i.e. 'external' magnetic field) to fit the Maxwellian boundary conditions. We will also discuss a possible 'active' normal electric field at MP (with a respective surface charge) later on in this section for a finite-gyroradius TCS with Hall conductivity. Those 'active' electric fields should result in extra re-configuration of inner and outer boundary layers for both high- and low-beta obstacles. As in our case outside MP the ion beta is not very high (~ 1.5-2), in the first approximation the stress of deformed magnetic field lines (i.e. a non-local factor) should be taken into account (cf. Dunlop et al., 2005). Returning to the magnetic field rotation in our case, we illustrate in Insert A of Fig. 2 that the mutual orientation of the ion flow velocity $\mathbf{V_i}$ (violet), magnetic field **B** (black) and MP in the unperturbed MSH flow: $\mathbf{V_i}$ and **B** are nearly parallel, conforming to the GDCF model predictions.

In Insert B we add the 'active' (i.e. visible in the MSH frame) normal electric field $\mathbf{E_n}$ (blue), that results mainly in the **B** rotation and in the $\mathbf{V_i}$ rise due to the cross-field drift (in case of Insert A the flow acceleration by $\mathbf{E_n}$ is impossible in the shown plane). Thus, the rise of the downstream flow velocity, seen in Fig. 5, should be the consequence not only of the $\mathbf{E_n}$ appearing, but also of the forced magnetic field rotation. Fig. 5 shows both quasi DC and wavy $E`_x$ (in the MSH frame) and $\mathbf{V_d}$. While the DC/wavy separation depends on the chosen upper frequency for the 'DC' processes, we believe that the evaluation, made in the previous section (for ~ 1/3 of the extra cross-field flow to be due to wavy disturbances) can be utilized for an order-of-magnitude estimate. Attributing the drift spikes to waves conforms to similar shapes of the dominant V_{dz} and P_z in the middle of Fig. 5 (i.e. the spikes of drift flow are not driven by cross-terms of DC and AC components in the fields' cross-product). Thus, the wavy input to the mass balance is secondary, but still substantial.

The difference outlined above in the sign of Y-components of the DC flow ($\mathbf{V_d}$) and wave propagation (Poynting vector **P**) in the middle of Fig. 5, indicates their inherent different physical nature. Positive P_x in similar wavy disturbances inside the jet under MP implies that the jet is a source for the waves in front of MP. Fluctuations of the surface charge and surface waves at TCS represent another possible sources, which are defined by the local shape of cusp throat, i.e. the sources should be the small-scale ones (i.e. of comparable scale with that of local curvature of the cusp throat). We illustrate the cusp throat configuration by sketches in Fig. 6: we overplot on the OVT (http://ovt.irfu.se/) magnetic field and spacecraft positions, the approximate MP (black lines at left side) and cusp throat (violet ellipse at right side) along with projections of different vectors, discussed earlier and further on; on the right-hand side also shown are the inferred plasma flow in the vicinity of the MP crossing by Clusters (curved arrow, bifurcated onto tailward streaming plasma and onto those one, entering the cusp throat - smaller arrow), and the possible location of anti-parallel large-scale reconnection at the dayside MP for the measured southward IMF (marked by circled "r"). The Poynting vector **P** (green) in the disturbance at ~ 20:00:40 UT is deflected toward the local normals $\mathbf{N_E}$ (blue, see [A]) and $\mathbf{N_B}$ (violet), the $\mathbf{V_d}$ is close to the model normal at smooth MP $\mathbf{N_{mod}}$ (gray, cf. Cargill et al., 2004). **P** departs only by 30 degrees from the full velocity of the jet under MP ($\mathbf{V_{jet}}$, black arrow), further confirming that the jet can irradiate the waves, carrying them downstream; the MP surface charges and/or waves would irradiate disturbances closer to the respective normals ($\mathbf{N_E}$, $\mathbf{N_B}$ or $\mathbf{N_{CTA}}$ - dark green, see upper panel of Fig. 6); an exclusion would be a surface wave, moving with group velocity ~

$\mathbf{V_{jet}}$, but in those cases the surface wave is the intermediate means for propagation of the sunward disturbance from the jet towards MSH.

Now we would like to discuss, why the normals $\mathbf{N_B}$ and $\mathbf{N_E}$ from minimum/maximum variance analysis with quite reasonable eigen values (see [A]) differ from each other and especially from the boundary velocities $\mathbf{V_{MP}}$ (red, from constant velocity approach – **CVA** (Haaland et al., 2004) - see Fig. 7 [A]), $\mathbf{N_{CTA}}$ and $\mathbf{N_{mod}}$ (see [A] and Cargill et al., 2004). Departure of the 'smooth' normal $\mathbf{N_{mod}}$ from the rest ones is accounted for the MP indentation over the cusp, which is due to a magnetic field minimum (see Dunlop et al., 2005, Chen et al., 1997, Savin et al., 1998, 2001 and 2004b, Boardsen et al., 2000 and Maynard, 2004), and the respective MP shape is depicted in Insert A of Fig. 6. The normal $\mathbf{N_E}$ has been calculated for the shortest time interval of several seconds, and thus it should be defined by the shortest-scale features, including the local normal to the funnel-like cusp throat with the negative N_{Ey} and positive N_{Ez}. Local surface waves can also substantially rotate the MP at those scales (cf. Cargill et al., 2004). However, 54 degrees between $\mathbf{N_E}$ and $\mathbf{N_{CTA}}$, calculated at the same time scales by different methods (cf. Dunlop et al., 2005), still requires an explanation as the former is repeated on 4 Clusters, the latter gives the MP thickness, confirmed by the cutoff in ion spectra on Cluster 1 and 3, and is thus fairly reliable. Note that $\mathbf{N_{CTA}}$ is really the direction of the MP velocity, which should hardly change much more than that of $\mathbf{N_E}$ on different Clusters (i.e. < 10 degrees). We do not think that such a difference can be uniquely due to a surface wave, as the similar difference (~ 25 degrees) is between $\mathbf{N_B}$ and $\mathbf{V_{MP}}$. Dunlop et al., (2005) for different time intervals obtain ~35 degrees between $\mathbf{N_B}$ and their 'timing' normal (i.e. **CVA**). We suggest that the MP movement at the cusp throat, where MP has the complicated shape, cannot be approximated by movement of any plane discontinuity and the MP velocity should not follow the local normal. I.e. in spite of local MP structure being well approximated by a plane surface (see also Dunlop et al., 2005), its movement is determined mainly by non-local properties of an extremely non-uniform magnetosphere in the outer cusp vicinity. We illustrate the suggestion by a simple example in Insert A of Fig. 6 by taking an indented boundary (lower curve) with violet spots for reference and simulating the MP compression (e.g. due to rising of the SW dynamic pressure) by diminishing its vertical size and enlarging the horizontal one to get the upper curve; then we shift the upper curve vertically until ~ coincidence of the shift direction of the upper violet spot (violet line) and the local normal (blue line). The latter takes into account the well-known fact that the dayside subsolar MP moves approximately along its normal (see e.g. Hultqvist et al., 1999). We do the horizontal enlargement because for the normal being close to X axis the shift of the boundary depends only on the magnetic field magnitude and its gradient (under MP boundary layer); in the subsolar region (upper part of Insert A) the magnetic field is > 100 nT and it sharply rises inside the magnetosphere, in our case $|\mathbf{B}|$ ~ 30 nT and it first drops just inside the MP (in 'plasma ball') and then rises moderately. So, the SW dynamic pressure rising can shift the trailing vertical wall of the cusp much farther than the subsolar MP. This simple consideration conforms to increasing cusp width with the SW dynamic pressure, reported by Van Allen and Adnan, (1992) from Hawkeye-1 data. For such boundary transformation, shift vectors of the reference spots in Insert A give a proxy for the MP velocity direction (violet lines). One can see that away from the MP indentation (upper and lower spots) the MP velocities and normals (blue lines) practically coincide, while in the middle the specific movement of MP as an entity results in the substantial departure of the two directions. Note the MP velocity proxy is close to the average normal. At the time of the MP encounter by Cluster (see upper side of Fig. 6) with the normal being close to X axis, the velocity also departs toward $\mathbf{N_{mod}}$, either $\mathbf{V_{MP}}$ or that of copied from Insert A. Thus, an oversimplified deformation model for the indented MP in Insert A provides a hint for an explanation of systematic departure of the normal from the MP velocity over cusp. We will make a quantitative test of our suggestion using a self-consistent gas-dynamic MSH/MP model in a future paper.

Returning to the difference of ~ 16 degrees between $\mathbf{N_E}$ and $\mathbf{N_B}$, the latter is turning towards $\mathbf{N_{mod}}$ as well (upper side of Fig. 6), because it has been calculated at 200 s intervals, which corresponds to scales of ~ R_E for the measured MP speed, i.e. the MP indentation/throat with typical scale of 2-3 R_E (cf. Savin et al., 1998, 2005a) is influenced less by the normal calculation at the larger scales. The same is applicable to $\mathbf{N_{CTA}}$ and $\mathbf{V_{MP}}$: the latter has been determined from 4-minute interval (Fig. 7 [A]) and it is much closer to $\mathbf{N_{mod}}$. As for $\mathbf{N_{CTA}}$, without a respective model we can only suggest similar behavior relative to that of $\mathbf{V_{MP}}$ (i.e. different direction of velocity and normal for a non-planar surface) and keep in mind a possible influence of dynamic behavior of moving MP, including local surface waves. A vector difference $\mathbf{(V_{CTA} - V_{MP})}$ fits a deceleration of the local flow in the large-scale MP frame in the direction normal to the cusp throat wall (see the XZ plane in Fig. 6), and to acceleration along the throat boundary (see the YZ plane in Fig. 6). The cusp throat appears to move with the average MP as a whole and to interact with local flows at the smaller scales. Note also, that any (originally) plane thin boundary, which moves along its average normal and has superimposed surface waves (either temporal or space ones), should display departures of local normals from the velocity direction (with maximum departures at places/times of the zero wave amplitudes).

The velocity of the jet inside TCS, $\mathbf{V_{jet}}$, occurring at 94 degrees to $\mathbf{N_B}$, departs from the velocity in MSH just prior to MP, $\mathbf{V_{MSH}}$ (yellow in Fig. 6) in XZ plane slightly towards -Z axis due to $\mathbf{V_{Djet}}$, driven by the negative E_x (Fig. 2) in the jet (which directs the stream around the obstacle), in YZ plane it departs towards -Y axis (a by-product of the negative

E_x, deflecting the flow away from the GDCF prediction), but the main effect is acceleration of the jet tailward. B_x and B_z in the jet change in opposite sense relative to both the inner magnetosphere and GDCF values (cf. Fig. 1 [A]), indicating rotation of the magnetic field to adjust to the electric field, 'fixed' at the TCS, similar to that of just outside MP. In fact, one can argue that the jet might be accelerated in the upstream outer cusp, e.g. due to an excess of the plasma pressure there, and both electric and magnetic fields are adjusting to the remote flow and local boundary conditions. But the parallel momentum transfer across the TCS (see Fig. 4 and the discussions above) requires generation of the respective local electric field. We have also demonstrated two different ion populations under MP (see Fig. 2 [A] and 6 [A] and discussions in [A]), which suggests a combination of local plasma penetration and that of remote one, including possible dayside anti-parallel reconnection (marked by the circled 'r' in YZ plane in Fig. 6). We have also mentioned that at the larger scales (see Fig. 2) the positive E_x outside MP should produce an extra surface charge at MP, which in turn requires the negative E_x inside MP (cf. e.g. Nikutowski et al., 1998). This opposite normal field inside MP (a consequence of Maxwellian boundary conditions) could have a rather general impact on the MP physics: independent of the origin of the induced electric field outside MP (i.e. independent of the correspondence with GDCF predictions in our case), just inside MP the opposite normal field should drive flow perpendicular to the local magnetic field. Thus, the transverse acceleration inside MP boundary layer (usually attributed to reconnection effects, cf. Hultqvist et al., 1999) can be an elelectrodynamic reaction on the external normal electric field. A future task is to check if electron field-aligned currents and other kinetic and dynamic effects can neutralize the inner electric field (cf. Genot et al., 2004), especially in the case of a dense inner boundary layer. In this dense layer any necessary 'active' surface charge can be easily provided by the field-aligned electrons (with electron density rising by tenths cm^{-3}), including that one supporting the non-GDCF positive E_x, which might serve to remove plasma in front of the moving MP (see Fig. 1 [A] and 2).

Another process with a possible 'active' role of the surface charge providing the MP current from the the Hall current at a TCS of finite-gyroradius scale required (by the magnetic field rotation). The Hall effect results from an electron current due to the cross-field drift of electrons, when a substantial part of the flow-carrying ions move in the direction of electric field (see e.g. Hultqvist et al., 1999 and Figs. 2 [A], 4 [A] and their discussion in [A]). An important issue is that the Hall effect and related thin electron currents are a characteristic feature for any current of ion finite-gyroradius scale independent of reconnection, which certainly should enlarge the mass and momentum transport, but it is not a necessary TCS feature.

Mozer et al., (2003) and Vaivads et al., (2004) provide comprehensive examples primarily for Hall dynamics in TCS from Polar and Cluster data. But they concentrated mostly on a comparison of the data with a limited stationary reconnection model with X-line, requiring a singular "diffusion region". This "diffusion region" should be very limited in space, including its length along MP. In contrast, the ion Hall effect in the thin current sheet should exist all along the sheet, unless the sheet width is comparable with ion gyroradius. In this case the frozen-in condition for ions is violated due to the small current scale, it could be also described in terms of an effective viscosity (see e.g. Stasiewicz, 1994). Belmont and Rezeau, (2001) show similar effects of Alfven waves on the magnetic flux erosion and use the term 'micro-reconnection' in contrast to a stationary laminar reconnection with the X-line configuration (see Hultqvist et al., 1999).

Thus we outline the Hall dynamics in TCS per se, while transient (and multiple) X-, Y-, O-lines etc. might be incorporated into a particular scenario of the current sheet evolution (see e.g. Syrovatskii, 1971, Hultqvist et al., 1999, Silin and Buechner, 2003, Savin et al., 2005a). To do a qualitative test particularly for Hall dynamics in the TCS in our case, we calculate the Hall term in the generalized Ohm law (see e.g. Hultqvist et al., 1999) using the data from Cluster 1 and inferred TCS geometry and velocity from 4 Clusters and compare its X-component with that of electric field:

$$\mathbf{[j \times B]}_x/en \sim -(B_z\, dB_z/dx + B_y\, dB_y/dx)/en \qquad (1)$$

where $\mathbf{j}$ - current density, n - plasma density from spacecraft potential with sampling 5 Hz, normalized by the WHISPER density data, e - electron charge. We have neglected all other gradients besides that in X-direction, as the normal $\mathbf{N_E}$ is close to the X axis, and the maximum variance procedure gives very different eigen values (i.e. the TCS can be regarded as a locally flat structure, cf. Dunlop et al., 2005, [A]). We also substitute $dx \sim V_x\, dt$, where the MP speed component V_x ~ 25-30 km both from $\mathbf{V_{MP}}$ and $\mathbf{V_{cta}}$ (see section 'MP thin current as plasma separatrix' in [A]). The result inside TCS is depicted in Fig. 7 (cf. upper plot in Fig. 8 [A]) by thick green line: in the middle of the TCS one can see that the spike in $\mathbf{[j \times B]}_x/en \sim E_x$ (now in the spacecraft frame, unlike Fig. 5), while at its borders the electric field matches the outer values, i.e. the boundary conditions, required for driving the respective frozen-in plasma jets outside the TCS (see Fig. 1-3 and related discussion above). I.e. with the available time resolution we can infer rather space than surface electron charge into the TCS, which serves both to support the necessary separating current via the Hall effect, and to fit the surrounding flows and fields, including the MP motion. Remembering the variability of magnetic disturbances near TCS on different spacecraft (Fig. 8 [A]) introduces extra uncertainty in calculating of the

Hall-term; we also take into account the geometrical and single-spacecraft limitations in our calculations of the Hall term. Then we can infer fairly satisfactory fitting of the data to the Hall physics in the center of the TCS. We have checked, that the E_x almost does not depend on transformation in frames, moving at speeds $\mathbf{V_{MP}}$ or $\mathbf{V_{cta}}$.

Dunlop et al., (2005) utilize the magnetic data from all spacecraft to calculate the current by the curlometer technique, while for the separatrix under study the inter-spacecraft distance of ~ 600 km is much larger than that of its width of ~ 100 km. They introduce the reverse cause and effect relation, proposing that the magnetic stress **[j x B]** at MP can accelerate the jet just inside MP dawnward, i.e. the stress could play an 'active' primary role. We argue that it should be the second-order effect, remembering the large ion β, which is especially high in the 'plasma ball'; while certainly the decisive role of the electric forces and surface charges, advocated here, may be confirmed in an appropriate modeling in future.

The potential difference for driving electron current along field lines can be provided by inertial (polarization) drift of the incident MSH ions in the non-uniform electric field of the surface charge, seen in the frame of bulk motion by the MSH plasma (see Fig. 2, 5, cf. Genot et al., 2004, Savin et al., 2005b). For a non-uniform electric field the zero approximation of the electric field cross-field drift with velocity $\mathbf{V}_d^{(0)} = c[\mathbf{E}\times\mathbf{B}]$ (*c* -speed of light, **E** and **B** - electric and magnetic field vectors) is broken and one should take into account the first order inertial drift (Golant et al., 1977):

$$\mathbf{V}_d^{(1)} = Ze/(M\omega_H^2)\ d\mathbf{E}/dt \qquad (2)$$

where M, ω_H, Ze are respectively mass, cyclotron frequency and charge of the particles. This approximation is valid only for space scales larger than ion gyroradius and frequencies smaller than ion gyrofrequency. In the opposite limit for the small scales, electric field should accelerate the ions directly, providing the Hall electron current in transverse direction. Regarding the disturbances in the middle of Fig. 5, a characteristic velocity $\mathbf{V_{MP}}$ (~ 30 km/s, ignoring its departure from X axis) and |B| ~ 50 nT (see Fig. 1 [A] and 2), one can get the appropriate scaling for different ion energies; the proton gyrofrequency being ~ 0.75 Hz. As an example we take the E_x rise at 20:00:24-26 UT (see Fig. 5), then (2) gives $\mathbf{V}_d^{(1)}$ ~ 3 km/s; the respective maximum ion shift from electrons in X direction due to inertial drift L_i ~ 6 km (i.e. ~ few electron inertial lengths or that of gyroradii); the inferred structure scale d_p ~ 45 km that corresponds to gyroradius of ~ 500 eV protons, so that the drift approximation is valid only for the protons with smaller energy. The protons with higher energies should loose ~ 100 eV in the sunward directed electric-field pulse of finite-gyroradius scale. In another spike at 20:00:15 UT with the inferred width of ~ 60 km and total potential change ~ 180 V, the inertial drift effects are negligible as the spike switches on and off faster than proton gyroperiod. Protons with energy > 900 eV (gyroradius ~ 60 km) loose the total potential energy; that of ~ 200 eV (and less) with gyroradius ~ half of the pulse width do not change their energies as the loss at the leading front is ~ gain at the trailing one. From 200 to 900 eV the energy loss rises to 180 eV, so that the respective velocity dispersion should result in a space charge, presumably neutralized by the parallel electron currents (cf. Genot et al., 2004). This inferred interaction with the small-scale electric fields is similar to that of TCS, discussed in section 'Plasma inflow and momentum balance'. While some electric bursts, to which we attribute the potentials ~ 100 V, could be the temporary ones, the high correlation of the signals in Fig. 7 [A] (especially on Clusters 2-4, separations of which in the normal direction ~ TCS width) with the definite lags, suggests their spatial nature in the majority of cases.

During period of the strong sunward field at 19:55-20:00 UT (see Fig. 2, 5), the higher-energy protons meet several positive E_x -pulses, thus loosing several hundreds eV. As we have seen (Fig. 3), the ions with energy > 300 eV carry main flow near MP, so namely those ions are subjected to decelerating by the spikes in normal electric field. This interaction could also account for the density rise of the higher-energy ions in Fig. 2 after the disturbance in electric field ~ at 19:50 UT.

The velocity of inertial drift changes sign at positive and negative dE_x/dt (see (2)), being of the order of few km/s (maximum), i.e. its influence on the ion dynamics is negligible. Typical shift of ions from electrons due to the drift is 10-50 km, that infers a space charge at the edges of the smooth gradients in electric field with characteristic potential difference of several tens V (~ change of potential at these distances in the measured fields). Genot et al., (2004) simulated similar features of the inertial drift in a non-uniform field of a finite-amplitude Alfven wave, and have demonstrated that the ion space charge is neutralized by parallel electron currents, split into thin layers of electron-inertial size. Our characteristic potential differences are similar to that of the simulations, and possible energy gains in them can exceed the electron temperature. The latter should result in electron beams at super-thermal speeds, which in turn generate high-frequency waves up to plasma frequency; those waves are seen in WHISPER data on the top panel in Fig. 8, including trailing TCS edge. Correlation between positive $E`_x$ spikes (in the MSH frame, black curve) and the

plasma waves (~ in the middle of the Y axis) looks to be fairly satisfactory, taking into account that the parallel electron flows are defined by potential difference along particular field lines, i.e. they have non-local character in contrast to the local electric field and wave measurements. Another experimental support for the suggestion for the plasma-wave generation by the disturbed thin electron sheets follows from comparison of the top and bottom panels in Fig. 8. The bottom panel displays an index of variation as deduced from the DWP correlator measurements for the pre-set energy 40eV to 100eV. The index of variation quantifies the variance in the electron counting process; the values are normalised to the estimated count rate and a value of unity indicates the electrons are random Poisson distributed (i.e. undisturbed). We put a threshold of +/- 0.3, marked by horizontal lines on the bottom panel in Fig. 8 and obtain a correlation of better than 50% with wave spikes on the top panel in the band 20-60 kHz. A narrowness of the electron disturbances follows from the correlator sample group interval of 732 microseconds, which corresponds to 20 m (~ the Debye length) in the case of scaling by the MP speed of ~ 30 km/s, and to 200 m for that of the MP jet (cf. Fig. 1 [A]). The scales of electron disturbances look to be underestimated on the background of electron inertial length and gyrogadius being of few km, but certainly these scales are much shorter than the characteristic ion ones.

So, our considerations suggest that in front of MP the sunward electric field in MSH frame: (i) by its DC component rotates magnetic field and accelerates the flow downstream along MP; (ii) by its spikes and gradients decelerates the higher-energy ions and produce space charges, most probably neutralized by parallel electron flows. Thus, we propose that the smaller-scale electric fields provide a kind of effective collision process for decreasing the average normal flows in the MP vicinity. Equalizing of the parallel and perpendicular ion temperatures in the zones of intensive electric fluctuations (Fig. 1 [A]) along with the temperature rise in front of MP, conforms to the hypothesis of effective collision operations. Another consequence of the effective collisions should be heating of O+ in the outer magnetosphere where its larger gyroradius should provide the more effective interaction with the short-scale electric bursts, compared to protons. In the presence of a surface charge O+ should be accelerated while moving in the DC electric field direction outward; we will discuss those points in details in a future paper.

Discussion and conclusions

The Hall effect at such thin charged layers, as the TCS discussed above, separating different plasmas, can serve to support the transverse current between the plasmas self-consistently (i.e. without any 'anomalous' resistivity or a 'diffusion region'). It does not necessarily imply 'classic' reconnection with parallel electric field, while reconnection should include the ion-scale layers. In other words, a charged TCS just because of its ion-gyroradius width becomes partially transparent for the larger-energy ions and respective magnetic flux without any change of the flow topology (which could be superimposed or not, cf. Moser et al., 2003). Transport of momentum across the layers is also provided by ions with larger gyroradius without any magnetic field annihilation. The momentum transfer has been discussed by Stasiewicz (1994) in terms of gyro-viscosity, which in the case of anti-parallel fields predicts a forcing of the boundary Earthward without a macro-reconnection. The ratio of the normal to MP gyro-viscous stress to Maxwell stresses is ~ $\beta\rho_u/2d$, where ρ_u is directional gyroradius and d , the MP width. Over the cusp and especially at the boundary of 'plasma balls' both β and ρ_u are rising due to the magnetic field minimum and due to the acceleration of the flow around MP towards the tail; thus, the MP inward motion due to this effect should have a maximum at the sunward edge of the cusp for the IMF $B_z < 0$ in our case (while Cluster entered the cusp at its tailward edge). In spite of sampling of the MP outside the maximum gyro-viscosity effect, predicted by Stasiewicz et al., (1994), Fig. 3 demonstrates clear momentum transfer across the MP, especially in its component, parallel to MP.

We have discussed that the ion inertial drift in the electric fields at TCS results in charge separation, probably neutralized by parallel electron currents, and the instability of which produces transverse electron scales (cf. Genot et al., 2004). In this case, the cascading towards electron scales should provide a similar measurement pattern, as supposed, but never clearly demonstrated, for the 'diffusion region' of 'classic' reconnection. So, we are skeptic about recent 'discoveries' of the 'diffusion regions' (see e.g. Moser et al., 2003 and references therein): the electron scales are mandatory for the localized 'diffusion region', but their presence all along a thin MP does not necessarily imply the boundary topology change and release of magnetic energy, stored in the deformed field. We plan to check our suggestion of the appearance of electrons scaled as a consequence of the inertial drift by respective modeling in a future paper.

This experimental case study has highlighted the fundamental role of a nonlinear decay of the flow disturbances into jets over the high-latitude MP in the cusp vicinity, where the plasma beta is high, the flow disturbances appear to produce both accelerated jets - up to magnetosonic speed -, and decelerated Alfvenic flows (Savin et al., 2004a, 2005b). The dynamic pressure in the jets is extremely large in comparison with the magnetic pressure in the nearby MP, which

makes it unlikely that they can have a reconnection origin. This implies that such jets could provide an input into the jets, discussed in this paper. Preliminary inspection of the upstream MSH data on February 13, 2001 confirms the existence of such anticipated jets. In the direct plasma-plasma interaction, the turbulent boundary layer presents an effective "obstacle" for the external flow (Savin et al., 2005a). As described above, the small-scale transverse electric fields decelerate the incident flow, being equivalent to "effective collisions". These effective collisions in the extended turbulent zones are a promising alternative in place of the usual parallel electric fields invoked in the macro-reconnection scenarios.

We would like to emphasize that the intrinsically non-stationary and non-uniform plasma jetting and related wave cascades, could be a fundamental plasma property, which may constitute an alternative to the laminar streamlining of a plasma around an obstacle: Savin et al. (2004b) suggested that the super-Alfvenic flow at high latitudes can be meta-stable, when magnetic stress balance cannot be fulfilled**,** and thus the magnetic field contains a larger amount of energy. In this maser-like approach the sonic jets resemble 'phonons', irradiated by the system to transfer into a stable state with minimum energy.

Finally, the study of nonlinear dynamics of the plasma flow interaction with the geomagnetic trap highlights a fundamental role of the finite-gyroradius effects, surface charges and accelerated plasma jets. In the MP boundary layers the accelerated jets provide a non-local flow balance via the 'active' electric field, most probably supported at the moving and indented MP by parallel electron currents, and via the respective rotation of magnetic field. The complicated MP shape suggests its systematic velocity departure from the local normal towards the average one. The electric fields in the MSH frame both accelerate the MSH plasma along MP downstream and provide effective collisions for reducing the MSH normal flows just in front of MP. The effective collisions should result in the ion heating and acceleration/deceleration, i.e. acquisition of the transverse electric potential by the higher energy ions.

ACKNOWLEDGMENTS
Work was partially supported by INTAS-03-50-4872

REFERENCES

Amata, E., S. Savin, … et al., this issue, (2005, cited as '[A]')
Andre, M., A. Vaivads, S. C. Buchert, A. N. Fazakerley, and A. Lahiff, Thin electron-scale layers at the magnetopause, *Geophys. Res. Lett.*, *31*, L03803, doi:10.1029/2003GL018137, (2004)
Belmont, G. and L. Rezeau, Magnetopause reconnection induced by Hall-MHD fluctuations, *J. Geophys. Res.,* **106** (A6), 10,751-10,760, (2001)
Boardsen, S. A.; Eastman, T. E.; Sotirelis, T.; Green, J. L., An empirical model of the high-latitude magnetopause, J. Geophys. Res., **105**, 23193-23220, (2000).
Cargill, P. J., M.W. Dunlop, B. Lavraud, R. C. Elphic, D. L. Holland et al., CLUSTER encounters with the high altitude cusp: boundary structure and magnetic field depletions, *Ann. Geophys*., **22**, 1739-1754, (2004)
Chen, S.-H., S. A. Boardsen, S. F. Fung, J. L. Green, R. L. Kessel, L. C. Tan, T. E. Eastman, and J. D. Craven, Exterior and interior polar cusps: Observations from Hawkeye, *J. Geophys. Res.,* **102**(A6), p. 11335, (1997)
Dunlop, M. W., B . Lavraud, P. Cargill, M. G. G.T. Taylor, A. Balogh et al., CLUSTER OBSERVATIONS OF THE CUSP: MAGNETIC STRUCTURE AND DYNAMICS , *Surveys in Geophys.,* **26**, No. 1-3 , 2005)
Genot, V.; Louarn, P.; Mottez, F., Alfven wave interaction with inhomogeneous plasmas: acceleration and energy cascade towards small-scales, Annals Geophys., ***22,*** 2081-2096, (2004)
Golant, V. E., Zhilinski, A. P., Sakharov, S. A., Basic Plasma Physics,, M., Atomizdat, pp. 245-248, (1977)
Haaland, S. E., B. U. ¨O. Sonnerup, M.W. Dunlop, A. Balogh, E. Georgescu et al., Four-spacecraft determination of magnetopause orientation, motion and thickness: comparison with results from single-spacecraft methods, *Ann. Geophys*., **22**, 1347–1365, (2004)
Haerendel, G., Microscopic plasma processes related to reconnection, *J. Atmos. Terr. Phys.,* **40**, pp. 343-353 (1978)
HULTQVIST, B., OIEROSET, M., PASCHMANN, G., TREUMANN, R., MAGNETOSPHERIC PLASMA SOURCES AND LOSSES, KLUWER ACADEMIC PUBLISHERS, DORDRECHT / BOSTON / LONDON, **INTERNATIONAL SPACE SCIENCE INSTITUTE,** Space Sciences Series of ISSI, pp. 207-353, (*Space Science Reviews,* **88**, Nos. 1- 2), (1999)
Lavraud, B., Dunlop, M. W., Phan, T. D., Reme, H., Bosqued, J. M., Dandouras, I., Sauvaud, J. A., Lundin, R., Taylor, M. G. G. T., Cargill, P. J., Mazelle, C., Escoubet, C. P., Carlson, C. W., McFadden, J. P., Parks, G. K., Moebius, E.,

Kistler, L. M., Bavassano-Cattaneo, M. B., Korth, A., Klecker, B. and Balogh, A., "Cluster observations of the exterior cusp and its surrounding boundaries under northward IMF", Geophys. Res. Lett., **29**, No. 20, 1995, (2002)
Lavraud, B., Rиme, H., Dunlop, M. W., Bosqued, J. M., Dandouras, I., Sauvaud, J.-A., Keiling, A., Phan, T. D., Lundin, R., Cargill, P., Escoubet, C. P., Carlson, C. W., McFadden, J. P., Parks, G. K., Moebius, E., Kistler, L., Amata, E., Bavassano-Cattaneo, M.-B., Korth, A., Klecker, B. and Balogh, A., "Cluster observes the high altitude / exterior cusp regions", *Surveys in Geophys.,* **26**, No. 1-3 , 2005
Maynard, N.C., Coupling of the solar-wind/IMF to the ionosphere through the high latitude cusps, *Surveys in Geophys.,* **26**, No. 1-3 , 2005
Mozer, F. S., T. D. Phan, and S. D. Bale, The complex structure of the reconnecting magnetopause, Phys. Plasmas, 10, doi:10.1063/1.1570419, 2480, (2003).
Nikutowski B., J.Buchner, H.Wiechen, U.Auster, K.H.Fornacon, J.Rustenbach, S.Klimov and S.Savin, A high-latitude boundary layer crossing - INTERBALL measurements and MHD model results, *Adv. Space Res*., **22**, N1, 161-165, (1998).
Nikutovski B., J.Buechner, S.Klimov, A.Petrukovich, S.Romanov, S.Savin**,** INTERBALL observations of field aligned current signatures due to collisionless reconnection, In *VIIth International Conference on Plasma Astrophysics and Space Physics,* Eds. J.Buchner, I.Axford,E.Marsch, V.Vasyliunas, Kluwer AP, Dordrecht, 687-692, (1999)
Savin, S. P., Borodkova, N. L., Budnik, E. Yu., Fedorov, A. O., Klimov, S. I. et al., Interball tail probe measurements in outer cusp and boundary layers, in *Geospace Mass and Energy Flow: Results from the International Solar-Terrestrial Physics Program*, edited by J.L. Horwitz, D.L. Gallagher and W.K. Peterson, Geophysical Monograph **104**, American Geophysical Union, Washington D.C., pp. 25-44, (1998)
Savin S.P., Zelenyi, L.M., Romanov, S.A., Klimov, S.I., Skalsky, A.A. et al., Turbulent Boundary layer at the Border of Geomagnetic Trap, *JETP Letters*, **74**, No 11, pp. 547- 551, (2001)
Savin S., Buechner, J., Consolini, G., Nikutowski, B., Zelenyi, L., Amata, E. et al., On the properties of turbulent boundary layer over polar cusps, *Nonlinear Processes in Geophysics*, **9**, 443-451, (2002)
Savin S.P., Zelenyi, L.M., Amata, E. et al., Dynanic Interaction of Plasma Flow with Hot Boundary Layer of Geomagnetic Trap, *JETP Letters*, 79, 452-456, (2004a)
Savin, S., L. Zelenyi, S. Romanov, I. Sandahl, J. Pickett, E. Amata, et al., Magnetosheath - Cusp Interface, *Ann. Geophys.*, **22**, 183-212, (2004b).
Savin, S., Skalsky, A., Zelenyi, L. Song, P., Fritz , T.A., Amata, E., Buechner, J. Blecki, J. et al., MAGNETOSHEATH INTERACTION WITH HIGH LATITUDE MAGNETOPAUSE, *Surveys in Geophys.,* **26**, No. 1-3 , 2005a
Savin, S., L. Zelenyi, E. Amata, J. Buechner, J. Blecki, A. Greco, S. Klimov, R.E. Lopez, B. Nikutowski, E. Panov *et al.*, Magnetosheath interaction with high latitude magnetopause: dynamic flow chaotization, Planet. Space Sci., **53**, 133-140, (2005b)
Scudder, J. D., Mozer, F.S., Maynard, N.C. and Russell, C.T., "Fingerprints of collision-less reconnection at the separator, I, Ambipolar-Hall signatures", *J. Geophys. Res.* **107**, (A10), Art. No. 1294, 2002.
Silin, I., J. Buechner, Nonlinear instability of thin current sheets in antiparallel and guided magnetic fields, *Phys. Plasma,* **10**, No. 9, 1-10, (2003)
Song, P., C. T. Russell, T. I. Gombosi, J. R. Spreiter, S. S. Stahara, and X. X. Zhang, On the processes in the terrestrial magnetosheath, 1: Scheme development*, J. Geophys. Res.,* **104**, 22,345, (1999)
Stasiewicz, *K.* (1994) Finite Larmor radius effects in the magnetosphere, Space *Sci.* Rev. **65,** 221.
Syrovatskii, S.I. Formation of current sheets in a plasma with a frozen-in strong magnetic field, *Sov. Phys. JETP,* **33**, 933-40, 1971.
Taktakishvili , A., Greco, A., Zimbardo, G., Veltri, P., Cimino, G., Zelenyi, L. and Lopez, R. E., THE PENETRATION OF IONS INTO THE MAGNETOSPHERE THROUGH THE MAGNETOPAUSE TURBULENT CURRENT SHEET, *Ann. Geophys.*, **21**, 1965 - 1973, (2003)
Vaivads, A.; Khotyaintsev, Y.; Andrй, M.; Retinт, A.; Buchert, et al., Structure of the Magnetic Reconnection Diffusion Region from Four-Spacecraft Observations, Phys. Rev. Lett. **93**, 105001 (2004)
Van Allen, J. A.; Adnan, J., Observed currents on the earth's high-latitude magnetopause, J. Geophys. Res., **97**, 6381-6395. (1992).
Zelenyi L.M., D. C. Delcourt, H. V. Malova and A. S. Sharma, "Aging" of the magnetotail thin current sheets, *Geophys. Res. Lett*., **29**, No. 12, 10.1029/2001GL013789, (2002)

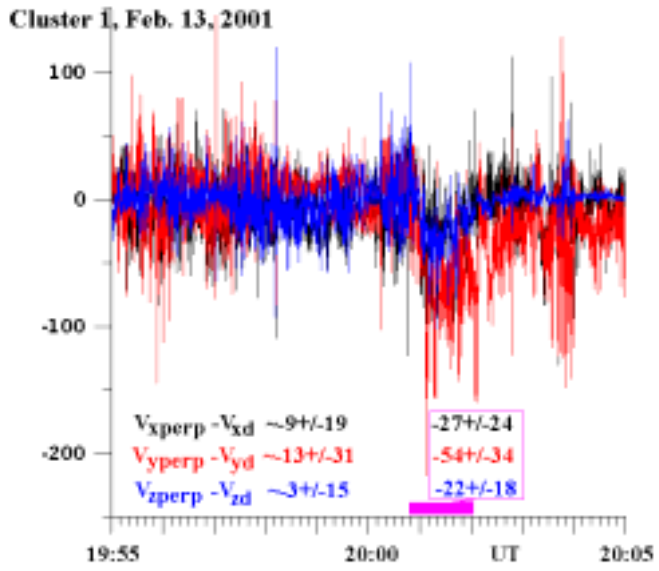

Fig. 1. Difference in [km/s] between the ion perpendicular velocity and electric drift velocity $\mathbf{V_{perp}-V_d}$. At the bottom are given average values and standard deviations for total interval (at the left) and for the jet under MP at 20:00:50-20:02:00 UT (at the right, marked by the violet bar), for which $|\mathbf{V_{perp}-V_d}|$~ 64 +/-45 km/s, i.e. ~31% of the total ion velocity at this interval. Inside magnetosphere at 20:04-20:05 UT the $V_{yperp}-V_{yd}$ ~ -20 +/-14 km/s is due to different offset in E_x component of electric field instrument (at 19:55:00-20:00:40 UT $V_{yperp}-V_{yd}$ ~3 +/-19 km/s).

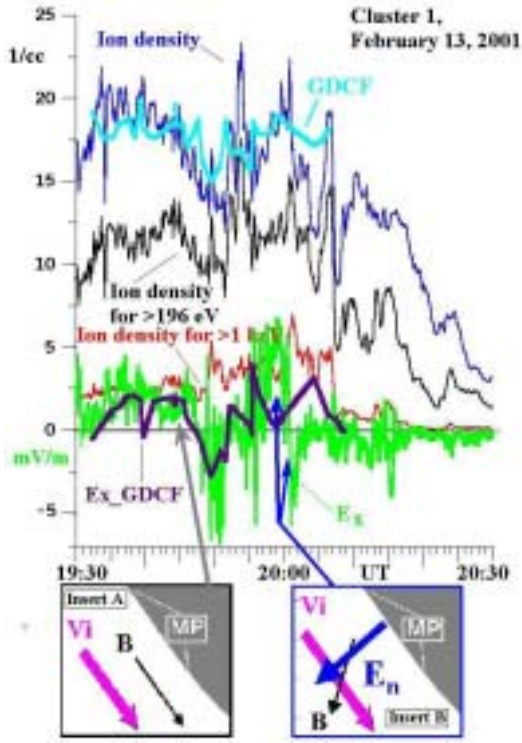

Fig. 2. Cluster-1, February 13, 2001. Top panel: Ion density (blue) near the MP entry (~ 20:01 UT); that of model GDCF (light blue), for ions with energy > 196 eV (black), > 1 keV (brown); electric field component E_x in spacecraft frame (green) and that of GDCF (thick superimposed line).
Bottom inserts: Insert A – scheme for ion velocity V_i (violet arrow) and magnetic field (black arrow) in unperturbed flow around MP, electric field in the flow

frame is negligible; Insert B – that of the flow, disturbed by the 'active' DC electric field (marked by 'E_n', blue arrow) along the MP normal, note rotation of the magnetic field and acceleration of the flow.

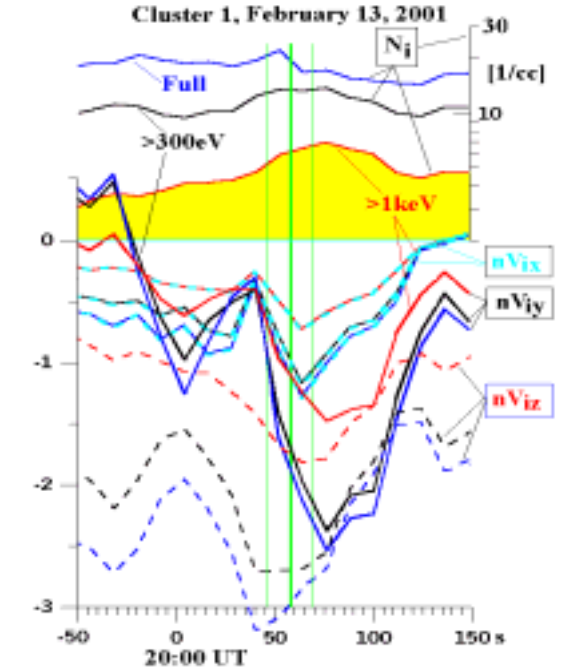

Fig. 3. Cluster-1, February 13, 2001. Top panel: Ion density N_i (blue), partial ion density for energies > 300 eV (black) and that of > 1 keV (violet, yellow shaded). Bottom panel: partial ion flux 'nV_i', dashed lines – z-component, full lines – y-component, full lines with light blue dashes – x-component; blue lines – full CIS energy range (see [A]), black – for > 300 eV, red – for > 1keV ions.

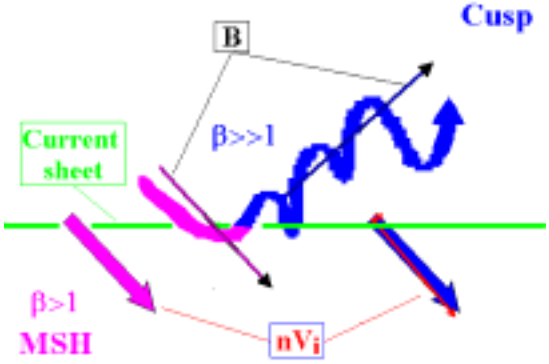

Fig. 4. Scheme for conservation of momentum (proportional to the ion flux nV_i, shown by thick arrows) by the ions with gyroradius larger than the MP width. While 'jumping' from MSH (over the figure plane, violet color, magnetic field (thin arrows) is ~ parallel to nV_i) into cusp (under the figure plane, blue color) the ions ~ conserve their momentum (for ion $\beta>1$) and start to rotate in the ~ perpendicular inner field. As a result, the magnetic field in the cusp with 'weak' energy density should be transported by the penetrated ions, i.e. in the cusp frame respective electric field will be generated to provide respective cross-field drift (see details in text).

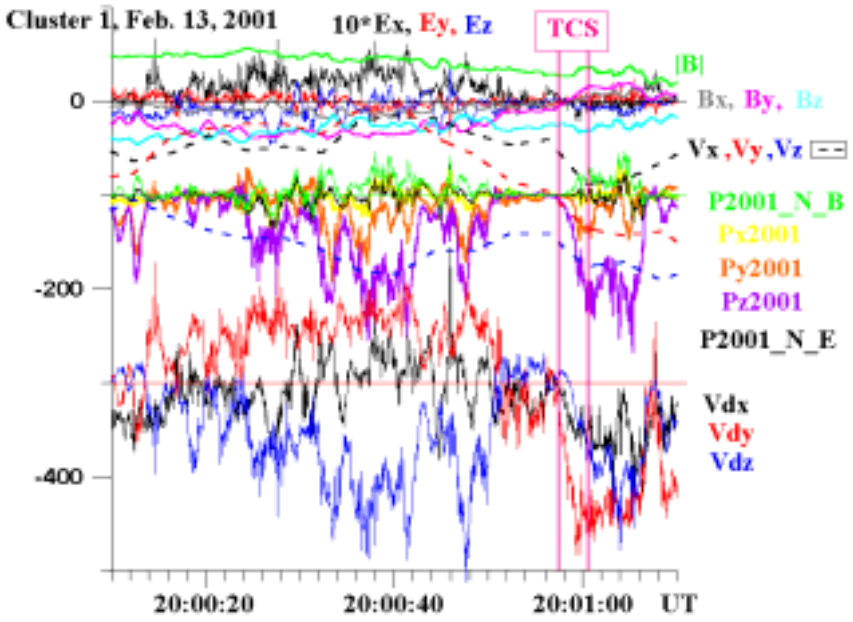

Fig. 5. Cluster-1, February 13, 2001. From the top (color coding for components is given in the middle or at the right side): GSE vector of electric field (**E**, multiplied by a factor 10) in a MSH-flow frame with $\mathbf{V_{MSH}}$ = (-45, -90, -150) km/s, taken just in front of the TCS (marked by 2 vertical lines); magnetic field vector and magnitude and ion velocity vector (dashed lines; shifted by -100 units, zero line is marked by green color); Poynting flux (**P**2001 in $\mu W/m^2$) GSE components, calculated from electric and magnetic field cross-product after subtracting of signal, averaged by the spline procedure with 2001 points of the interpolated data with sampling at 25 Hz; P2001_N_B green line - Poynting flux along the average normal from magnetic minimum variance analysis $\mathbf{N_B}$ (see Cargill et al., 2004), P2001_N_E - the same along electric field direction of maximum variance $\mathbf{N_E}$, shifted by -300 units (zero line is marked by red color, see [A]); and, finally, the vector of electric drift-velocity ($\mathbf{V_d}$, also shifted by -300 units)

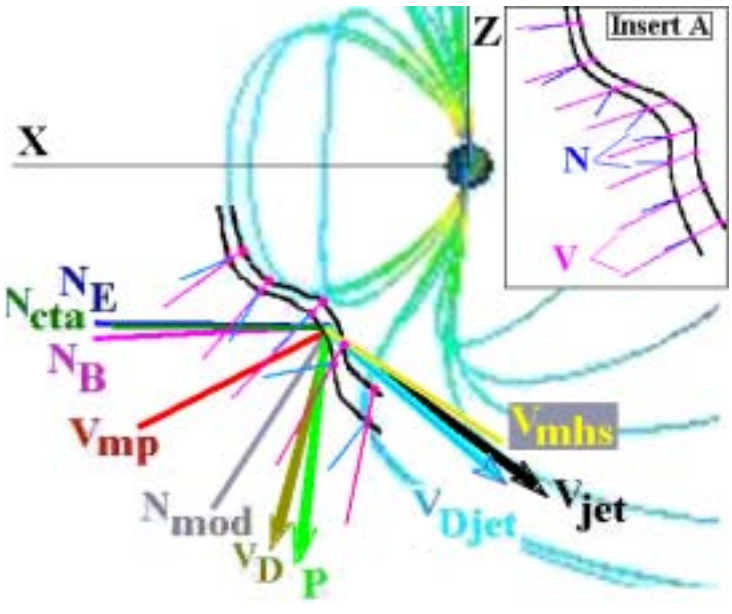

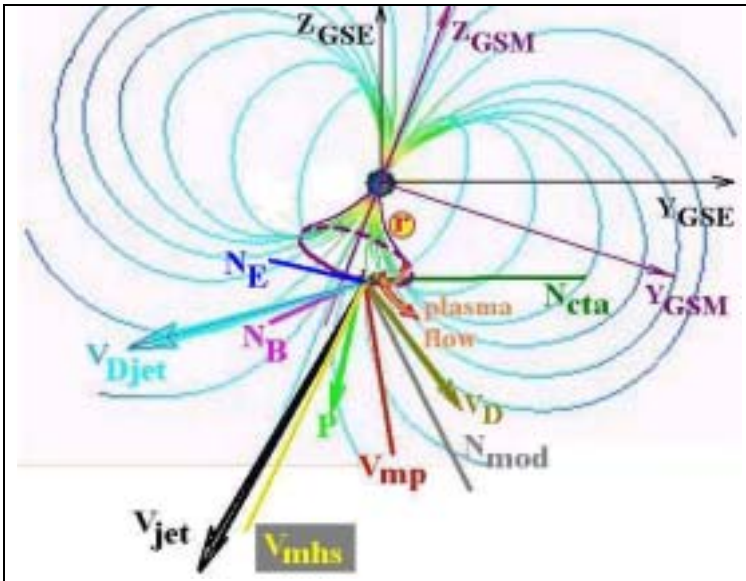

Fig. 6. Model magnetic field lines and direction of different vectors in the MP vicinity (see text) for inbound crossing of Clusters on February 13, 2001. Upper panel – XZ GSE plane with Insert A (a cartoon for MP deformation, see details in the text). Lower panel – YZ GSE plane (Z and Y in GSM are superimposed);

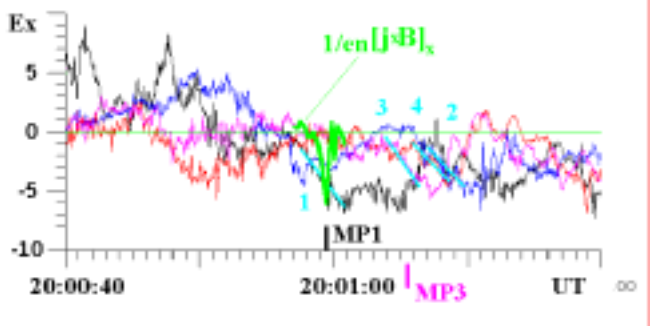

Fig. 7. GSE electric field component E_x in spacecraft frame (cf. Fig. 7 in [A], upper panel), color-coded for Cluster 1 through 4 as black, blue, violet and red. By the thick green line we superimpose $[jxB]_x/en$ calculated from (1) on Cluster-1 in the MP vicinity. Se text for details.

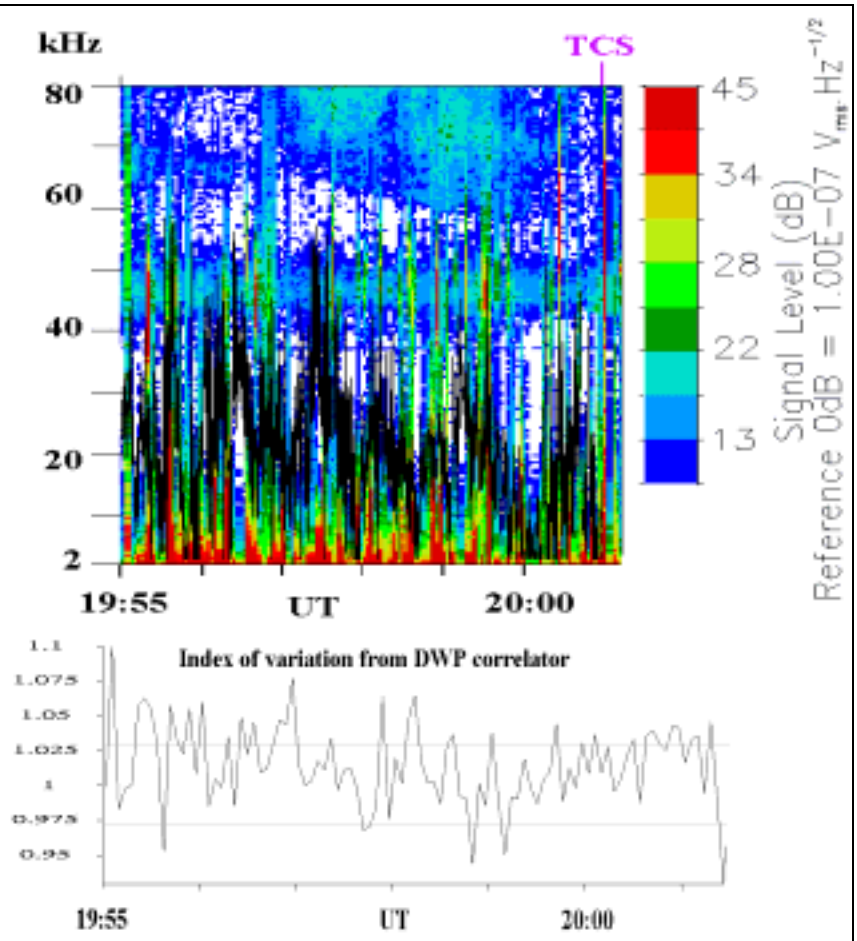

Fig. 8. Cluster-1, February 13, 2001. Top panel: WHISPER electric field spectrogram (see [A]) with color-coded intensity (scale at the right side). By black line electric field positive values of $E`_x$ in the MSH frame are superimposed (from Fig. 5)
Bottom panel: Index of variation as deduced from the DWP correlator measurements for the pre-set energy (i.e. 40eV to 100eV), which quantifies the variance in the electron counting process that the DWP correlator performs. The values are normalised to the electron count rate and a value of unity indicates the electrons are random Poisson distributed.